INL/EXT-17-42125

Preliminary Two-Phase Terry Turbine Nozzle Models for RCIC Off-Design Operation Conditions

Haihua Zhao
James O'Brien

June 2017

U.S. Department of Energy Office of Nuclear Energy

INL/EXT-17-42125

Preliminary Two-Phase Terry Turbine Nozzle Models for RCIC Off-Design Operation Conditions

Haihua Zhao, James O'Brien

June 2017

Idaho National Laboratory
Idaho Falls, Idaho 83415

http://www.inl.gov

Prepared for the
U.S. Department of Energy
Office of Nuclear Energy
Under DOE Idaho Operations Office
Contract DE-AC07-05ID14517

EXECUTIVE SUMMARY

As part of the efforts to understand the unexpected "self-regulating" mode of the RCIC (Reactor Core Isolation Cooling) systems that was observed during the Fukushima accidents and to extend BWR RCIC and PWR AFW (Auxiliary Feed Water) operational range and flexibility, mechanistic models for the Terry turbine are being developed and tested with the RELAP-7 code to simulate the RCIC system. In previous work, we developed a set of analytical models [1] for the normal working conditions of the RCIC system, based on Sandia's original work [2]. In this set of models, we proposed an alternative method, using an under-expanded jet model to replace the CFD-based reduced-order model in the Sandia work to obtain the velocity and thermodynamic conditions for the turbine stator inlet. The models include both an adiabatic expansion process inside the nozzle and a free expansion process outside of the nozzle to ambient pressure. The newly developed nozzle models and the modified turbine rotor model according to the Sandia's original work were tested with RELAP-7, along with the original Sandia Terry turbine model. A new pump model was also developed and implemented to couple with the Terry turbine model. An input model was developed to test the Terry turbine RCIC system, which generates reasonable results.

This report presents the effort to extend the single-phase analytical Terry turbine model to cover two-phase off-design conditions. The work includes: (1) adding well-established two-phase choking models – the Isentropic Homogenous Equilibrium Model (IHEM) and Moody's model, and (2) theoretical development and implementation of a two-phase nozzle expansion model. The two choking models provide bounding cases for the two-phase choking mass flow rate. The new two-phase Terry turbine model uses the choking models to calculate the mass flow rate, the critical pressure at the nozzle throat, and steam quality. In the divergent stage, we only consider the vapor phase with a similar model for the single-phase case by assuming that the liquid phase would slip along the wall with a much slower speed and will not contribute the impulse on the rotor. We also modify the stagnation conditions according to two-phase choking conditions at the throat and the cross-section areas for steam flow at the nozzle throat and at the nozzle exit.

The new two-phase Terry turbine model was benchmarked with the same steam nozzle test as for the single-phase model. Better agreement with the experimental data is observed than from the single-phase model. We also repeated the Terry turbine nozzle benchmark work against the Sandia CFD simulation results with the two-phase model for the pure steam inlet nozzle case. The RCIC start-up tests were simulated and compared with the single-phase model. Similar results are obtained. Finally, we designed a new RCIC system test case to simulate the self-regulated Terry turbine behavior observed in Fukushima accidents. In this test, a period inlet condition for the steam quality varying from 1 to 0 is applied. For the high quality inlet period, the RCIC system behaves just like the normal operation condition with a high pump injection flow rate and a nominal steam release rate through the turbine, with the net addition of water to the primary system; for the low quality inlet period, the RCIC turbine shaft work dramatically decreases and results in a much reduced pump injection flow rate, and the mixture flow rate through the turbine increases due to the high liquid phase flow rate. The net effect for this period is net removal of coolant from the primary loop. With the periodic addition and removal of coolant to the primary loop, the self-regulation mode of the RCIC system can be maintained for a quite long time. Both the IHEM and Moody's models generate similar phenomena; however noticeable differences can be observed.

Due to funding and time constraints, the work discussed in this report only represents the first step preliminary models for simulating RCIC system off-design conditions. Many two-phase model options can be considered. The near future work should be focused on using Terry turbine test data to validate the proposed models when the data become available. Additional model refinement will also be pursued, such as trying other choking models and investigating different expansion models in the nozzle divergent section, adding homologous curves for the pump, and developing thermal mixing and stratification models for the wet well.

ACKNOWLEDGEMENTS

The funding for this project is provided by the Reactor Safety Technology Pathway of the Light Water Sustainability Program, U.S. Department of Energy.

CONTENTS

FIGURES

TABLES

ACRONYMS

0-D	zero-dimensional
BC	Boundary Condition
BWR	Boiling Water Reactor
FY	Fiscal Year
INL	Idaho National Laboratory
LWRS	Light Water Reactor Sustainability
RCIC	Reactor Core Isolation Cooling
RELAP-7	Reactor Excursion and Leak Analysis Program 7
PWR	Pressurized Water Reactor
SBO	Station Blackout
SRV	Safety Relief Valve

1. INTRODUCTION

As part of the efforts to understand the unexpected "self-regulating" mode of the RCIC (Reactor Core Isolation Cooling) systems in Fukushima accidents and extend BWR RCIC and PWR AFW (Auxiliary Feed Water) operational range and flexibility, mechanistic models for the Terry turbine, are being developed and tested with the RELAP-7 code to simulate the RCIC system. All BWR RCIC systems and PWR AFW systems use Terry turbines. The Terry turbine, as shown in Figure 1, is essentially a solid cylindrical wheel with multiple machined semi-circular 'buckets' that are shaped into the body of the wheel. Fixed nozzles and reversing chambers surrounding the wheel are inside the turbine casing. High pressure steam is accelerated to supersonic flow inside the turbine nozzle. The kinetic energy is then converted to shaft work by the impulse force on the turbine buckets.

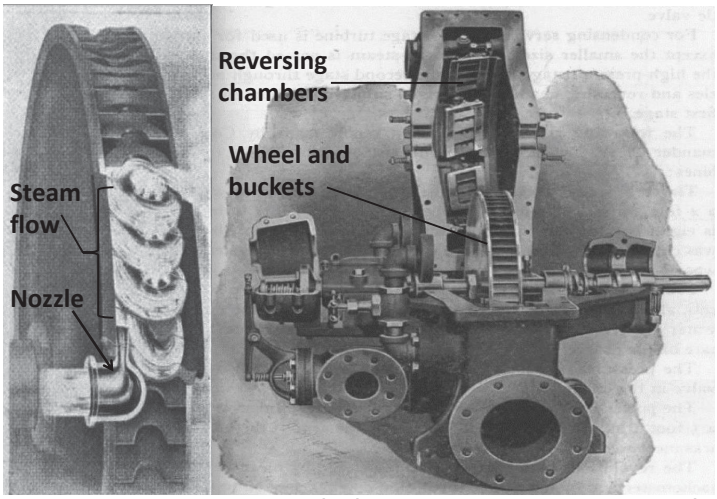

Figure 1. Terry turbine bucket flow (left) and interior view of turbine case (right) [2]

Prior to the Fukushima accidents, all the safety analyses assumed that the RCIC system couldn't work properly if the Terry turbine inlet is flooded. Under the normal operation condition, the water mass flow rate through the pump into the primary system is about 10 times the steam flow rate through the Terry turbine leaving the primary system. Therefore, battery power (can last from 4 to 12 hours) is required to control the RCIC system in order to prevent the reactor vessel water level from rising too high; otherwise loss of DC power would result in flooding of the steam lines and an assumed subsequent failure of the RCIC system [2 and 3]. In contrast, real-world observation from Fukushima Daiichi Unit 2 (1F2) shows that RCIC function was not terminated by uncontrolled steam line flooding, and instead continued providing water injection for nearly three days.

A set of Terry turbine models suitable for system code implementation was developed by Sandia National Labs in FY15 [2]. The Sandia Terry turbine model is based on the following assumptions:

- RCIC uses a single-stage Terry impulse turbine that functions according to the exchange of momentum and kinetic energy.
- Steam enters semi-circular buckets and reverses direction (~180°).
- The reversing chambers are only important for low-speed operation, such as during the initial startup.
- The expansion of steam downstream of the nozzles is total; the expansion process converts the static pressure (enthalpy energy) of the steam into kinetic energy to be imparted into the turbine buckets. No meaningful reaction force is developed by the Terry turbine.

The Sandia Terry turbine model is composed of a turbine nozzle model and a turbine rotor model. For the Sandia turbine nozzle model, the turbine bucket inlet velocity is provided according to a reduced-order model which was obtained from a large number of CFD simulations. This reduced-order model is only valid for the specific nozzle design and operation conditions for which the CFD simulations were performed.

In our previous work, we developed a set of analytical models [1] for the normal working conditions of the RCIC system, based on Sandia's original work [2]. In this new set of models, we proposed an alternative method, using an under-expanded jet model to replace the CFD-based reduced-order model in the Sandia work to obtain the velocity and thermodynamic conditions for the turbine stator inlet. The models include both an adiabatic expansion process inside the nozzle and a free expansion process outside of the nozzle to ambient pressure. The newly developed nozzle models and modified turbine rotor model according to the Sandia's original work were tested with RELAP-7, along with the original Sandia Terry turbine model. A new pump model was also developed and implemented to couple with the Terry turbine model. For brevity, we refer to the set of RELAP-7 RCIC models as INL RCIC model or INL model, which is composed of two parts:

- Nozzle model which predicts mass flow rate through the turbine and inlet conditions for the rotor (semi-circular buckets),
- Turbine rotor model which describes the balance of angular momentum of the wheel.

The INL model is able to predict the steam mass flow rate and supersonic velocity at the Terry turbine bucket entrance, which are the necessary input conditions for the Terry Turbine rotor model. The nozzle analytical models were validated with experimental data and benchmarked with CFD simulations. The analytical models generally agree well with the experimental data and CFD simulations.

This report presents the effort to extend the single-phase analytical Terry turbine model to cover two-phase off-design conditions. The work includes: (1) adding well-established two phase choking models - Isentropic Homogenous Equilibrium Model (IHEM) and Moody's model, and (2) theoretical development and implementation of a two-phase nozzle expansion model. All the models were tested with the RELAP-7 system analysis code and input models were also developed for benchmark, validation, and tests. The new two-phase Terry turbine model was benchmarked with the same steam nozzle tests as for the single-phase model. The RCIC start-up tests were simulated and compared with the single-phase model. Finally, we designed a new RCIC system test case to simulate the self-regulated Terry turbine behavior observed in Fukushima accidents. In this test, a period inlet condition for steam quality varying from 1 to 0 is applied.

Section 2 discusses the refined RCIC model for two-phase off-design cases. Section 3 presents the nozzle test, start-up test and the self-regulated RCIC working condition test. Section 4 summarizes the work and discusses additional work for the future.

2. TWO-PHASE TERRY TURBINE MODEL

2.1 Two-Phase Nozzle Model

The fluid from the turbine inlet is accelerated to the supersonic condition inside the nozzle and then further expands in the gap between the nozzle exit and turbine bucket inlet. The nozzle model covers both the nozzle internal expansion and free expansion out of the nozzle. Figure 2 shows that the single-phase gas jet flow through a convergent-divergent nozzle can be characterized with four distinct stages: (1) adiabatic expansion to sonic condition at the throat from the source and adiabatic expansion to supersonic condition in the divergent part of the nozzle; (2) adiabatic free expansion out of the nozzle to ambient pressure (virtual nozzle); (3) zone of flow establishment (ZOFE); (4) free jet. Different models are used for analyzing each stage. As discussed in our previous report [1], the jet is assumed to enter the bucket near the maximum speed, where the jet static pressure is equal to the turbine pressure. Therefore, the zone of flow establishment and free jet models are irrelevant in the simulation and are skipped.

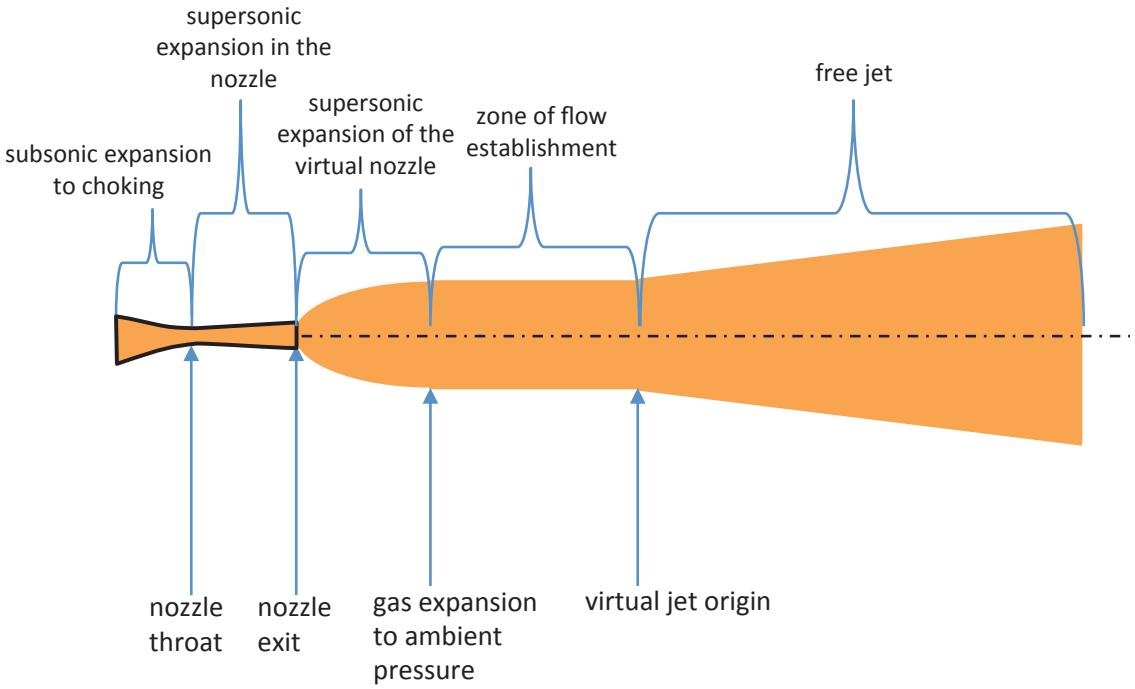

Figure 2. Schematic of high pressure gas flow through a nozzle.

We develop the two-phase Terry turbine nozzle model based on the single-phase nozzle model. It is very helpful to know the flow regimes inside a supersonic convergent-divergent nozzle. However, there are no direct measurement data available due to high pressure and high speed. It has been hypothesized [4 and 5] that bubbles form homogeneously in the decompression region near the pipe entrance, which leads to homogeneous critical flow condition. This condition is followed by phase separation with discharge in the annular or separated flow regime. This explains why IHEM can predict flows in terms of the upstream properties, and yet under-predict flows in terms of pipe discharge properties; slip flow models over-predict in terms of vessel properties, and yet accurately predict the flow based on pipe discharge properties. We develop a two-phase nozzle expansion model according to this hypothesis: the flow

regime is bubble flow in the convergent section and the flow regime transitions to slip flow in the divergent section, as shown in Figure 3. This new two-phase nozzle model uses classic choking models to calculate the mass flow rate, the critical pressure at the nozzle throat, and the steam quality. In the divergent section, we only consider the steam phase with the similar model as for the single-phase case by assuming that the liquid phase would slip along the wall with a much slower speed and will not contribute the impulse on the rotor. We also modify the stagnation conditions according to two-phase choking conditions at the throat and the cross-section areas for steam at the nozzle throat and at the nozzle exit. Therefore, the two-phase nozzle model consists of three parts: (1) choking model in the convergent section; (2) supersonic expansion model in the divergent section; and (3) free expansion model outside of the nozzle. The following subsections will describe the models in details.

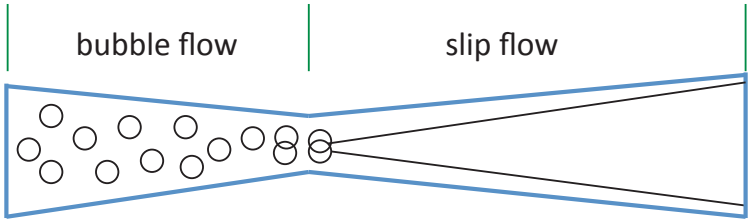

Figure 3. Two phase choking inside a convergent-divergent nozzle.

2.1.1 Choking Models

In this work, we only implemented the two most widely used choking models – IHEM and Moody's critical flow models. These two thermal equilibrium choking models provide bounding cases for the two-phase choking mass flow rate. The IHEM model predicts the lower bound value of the choked flow rates while Moody's model predicts the upper bound value [6]. More complex non-equilibrium choking models can be added later if necessary.

IHEM critical flow model

According to reference [6], this model assumes equal phasic velocities and thermal equilibrium between the phases. The properties of the homogeneous mixtures are

$$\rho = \left(\frac{1-x}{\rho_L} + \frac{x}{\rho_G}\right)^{-1} = \left[\frac{1}{\rho_L} + x\left(\frac{1}{\rho_G} - \frac{1}{\rho_L}\right)\right]^{-1} \tag{1}$$

$$h = h_L(1-x) + h_G x = h_L + x(h_G - h_L) \tag{2}$$

$$s = s_L(1-x) + s_G x = s_L + x(s_G - s_L) \tag{3}$$

$$x = \frac{\alpha\rho_G}{\alpha\rho_G + \rho_L(1-\alpha)} \tag{4}$$

where x is the equilibrium steam quality, ρ the density, h the enthalpy, s the entropy, α the void fraction, and subscripts L, G are used for liquid and gas, respectively.

According to energy conservation, for an upstream stagnant condition defined by the subscript 0, the mass flux can be calculated by

$$G = \left[2\left(h_0 - h(p,x)\right)\right]^{\frac{1}{2}}\rho(p,x) \tag{5}$$

Assuming an isentropic process,

$$s_0 = s(p, x) \tag{6}$$

We can derive

$$\mathrm{x} = \frac{s_0 - s_L(p)}{s_G(p) - s_L(p)} \tag{7}$$

$$\alpha = \frac{\rho_L x}{\rho_L x + \rho_G (1 - x)} \tag{8}$$

$$\mathrm{G_G} = \mathrm{xG} \tag{9}$$

$$\mathrm{u_G} = \frac{\mathrm{G_G}}{\alpha \rho_G} \tag{10}$$

Where α is the void fraction, and $\mathrm{u_G}$ the steam velocity.

The flow is choked whenever

$$\mathrm{G(p)} = G_{max} \tag{11}$$

Eq. (11) can be solved with the Golden Section Search algorithm [7] by following the method discussed in ref. [6]. The results are validated with Moody's IHEM critical mass flux and critical pressure figures.

Moody's Critical Flow Model

Moody's model assumes thermal equilibrium between the two phases but different phasic velocities. Define the slip ratio as

$$\mathrm{K} = \frac{u_G}{u_L} \tag{12}$$

The void fraction is

$$\alpha = \frac{\rho_L x}{\rho_L x + K \rho_G (1 - x)} \tag{13}$$

The mixture mass flux is

$$\mathrm{G} = \sqrt{\frac{2\left[h_0 - h_L - \frac{h_{LG}}{s_{LG}}(s_0 - s_L)\right]}{\left[\frac{K(s_G - s_0)v_L}{s_{LG}} + \frac{(s_0 - s_L)v_G}{s_{LG}}\right]^2 \left[\frac{s_0 - s_L}{s_{LG}} + \frac{s_G - s_0}{K^2 s_{LG}}\right]}} \tag{14}$$

Where v is the specific volume; subscript LG indicates the latent properties. To maximize G, it must satisfy the following conditions:

$$\left(\frac{\partial \mathrm{G}}{\partial \mathrm{K}}\right)_P = 0 \tag{15}$$

$$\left(\frac{\partial \mathrm{G}}{\partial \mathrm{P}}\right)_K = 0 \tag{16}$$

Eq. (15) leads to

$$K_M = \left(\frac{v_G}{v_L}\right)^{1/3} \tag{17}$$

Eq. (16) is also solved with the Golden Section Search algorithm [7].

2.1.2 Steam Supersonic Expansion Model

The steam supersonic expansion model assumes there is no phase change during the extremely fast transient in the divergent part of the nozzle. This approach is similar to the frozen model treatment in literature [6]. The steam expands by following an isentropic process. Mixture static temperature at the throat is given by:

$$T_t = T_s(p_t) \tag{18}$$

Where p_t is the throat pressure calculated by the choking model. Steam stagnation temperature at the throat is:

$$T_{0t} = T_t + \frac{a_{mt}^2}{2c_p} \tag{19}$$

Where a_{mt} is the mixture sound speed calculated by the choking model, and c_p is the specific heat at constant pressure for the steam. Steam stagnation pressure at the throat is calculated by:

$$p_{0t} = p_t \left(\frac{T_{0t}}{T_t}\right)^{\gamma/(\gamma-1)} \tag{20}$$

where γ is the specific heat ratio for steam. A modified throat area is used for steam flow only:

$$A_{tG} = \alpha_t A_t \tag{21}$$

Where α_t is the void fraction at the throat, which is calculated by the choking model, and A_t the nozzle cross-section area at the throat. Also modify the nozzle exit area for steam flow only:

$$A_{eG} = \alpha_e A_e \tag{22}$$

$$\alpha_e = \frac{\rho_L x_t}{\rho_L x_t + K\rho_G(1 - x_t)} \tag{23}$$

Where α_e is the void fraction at the nozzle exit, the slip ratio is 1 for IHEM model and is calculated by Eq. (17) for Moody's model. In Eq. (23), we assume a frozen model by assuming no further phase change downstream of the throat. The Mach number (M) at the nozzle exit can be calculated using the following equation [8]:

$$\frac{A_{eG}}{A_{tG}} = \left(\frac{\gamma+1}{2}\right)^{-\frac{\gamma+1}{2(\gamma-1)}} \frac{\left(1 + \frac{\gamma-1}{2}M^2\right)^{\frac{\gamma+1}{2(\gamma-1)}}}{M} \tag{24}$$

When Mach number is available, the pressure, temperature and density can be calculated according to the following equations, respectively:

$$\frac{p}{p_0} = \left(1 + \frac{\gamma-1}{2}M^2\right)^{-\frac{\gamma}{\gamma-1}} \tag{25}$$

$$\frac{T}{T_0} = \left(1 + \frac{\gamma-1}{2}M^2\right)^{-1} \tag{26}$$

$$\frac{\rho}{\rho_0} = \left(1 + \frac{\gamma - 1}{2} M^2\right)^{-\frac{1}{\gamma - 1}} \tag{27}$$

The sound speed is calculated as:

$$a = \sqrt{\gamma R T} \tag{28}$$

where R is the gas constant for steam. Velocity is calculated from:

$$u = Ma \tag{29}$$

With Eqs. (25) to (29), the flow conditions at the nozzle exit can be calculated.

2.1.3 Free Expansion Model

For the non-isentropic adiabatic free expansion process from the nozzle exit to ambient pressure, local pressure, temperature, velocity, and density vary rapidly while the jet diameter expands significantly over a short distance from the nozzle exit [9]. This process is called virtual nozzle in literature. The mass entrained by the jet during this expansion process is insignificant compared to the jet mass flow rate from the nozzle exit. Therefore, it is assumed that there is no mass flux through the jet boundary at this stage. According to mass, momentum, energy balances and the ideal gas law, four equations can be formulated to calculate jet velocity, temperature, density, and diameter at the end of this stage. This method has been used by Xiao et al. [10] and Bulent Yuceil [9]. The following summarizes the model:

$$u_v = \frac{p_e - p_v + \rho_e u_e^2}{\rho_e u_e} \tag{30}$$

$$T_v = T_e + \frac{u_e^2 - u_v^2}{2c_p} \tag{31}$$

$$\rho_v = \frac{\rho_e T_e}{p_e} \frac{p_v}{T_v} \tag{32}$$

$$d_v = d_e \sqrt{\frac{\rho_e u_e}{\rho_v u_v}} \tag{33}$$

Where subscript v represents the location at the end of the virtual nozzle and e represents the location at the nozzle exit, and d is the diameter.

In order to estimate the length of this stage, the distance for the Mach disk, where the shock occurs, is assumed to approximate this expansion length. The model developed by Velikorodny and Kudriakov [11] is used in this report to calculate the distance for the Mach disk:

$$\frac{x_v}{d_e} = \frac{1}{2} \sqrt{\frac{\gamma P_e}{P_\infty}} \left(\frac{\gamma + 1}{\gamma - 1}\right)^{1/4} \tag{34}$$

Given upstream conditions, this set of models calculates the Terry turbine bucket inlet conditions such as velocity and mass flow rate. These inputs are used to close the angular momentum equation for the turbine rotor.

2.2 INL Terry Turbine Rotor Model

As reported in our previous work [1], the Terry turbine rotor model developed by Sandia [2] has been adopted with only one modification for consideration of the angular momentum conversion efficiency. The angular momentum relationship on the turbine wheel control volume is used for the turbine rotational speed (ω):

$$I\frac{d\omega}{dt}+\frac{T_{pump}}{1+\cos\beta}=c_{IC}\left(2r\dot{m}V_j\frac{\cos\beta}{1+\cos\beta}-r^2\dot{m}\omega\right) \tag{35}$$

In Eq. (35), I is the turbine moment of inertia. T_{pump} is pump torque, which will be coupled from a pump model. β is the inlet/exit angle between the fluid velocity vectors and the horizontal/tangential direction of the turbine motion. c_{IC} is an impulse conversion coefficient for accounting for the efficiency to convert the fluid kinetic energy to the driving moment for the angular momentum. This is a new concept added to the original Sandia model. A coefficient model should be developed according to experimental results. $\dot{m}$ is the mass flow rate as calculated by Eq. (1). V_j is the nozzle jet velocity as calculated by the virtual nozzle exit velocity model (Eq. (30)).

The turbine shaft work supplied to the pump is calculated as

$$\dot{W}_t=T_{pump}\omega \tag{36}$$

2.3 INL Pump Model

The pump model for the RCIC system is based on two assumptions:

- quasi-steady state,
- incompressible flow,

We designed the pump as one 0-D junction component which provides:

- one BC for upstream pipe: pressure
- two BCs for downstream pipe: pressure and total energy.

Four scalar variables: pump pressure p_J, pump temperature T_J, pump head H, and pump torque T_{pump} are defined as the unknowns for the pump model.

The pump pressure unknown corresponds to the mass balance Eq. as the nonlinear equation:

$$(\rho uA)_1-(\rho uA)_2=0 \tag{37}$$

Where subscript 1 and 2 indicate inlet and outlet conditions.

The pump temperature corresponds to the pump energy conservation equation:

$$\left(E+\frac{p}{\rho}\right)_2(\rho uA)_2=\left(E+\frac{p}{\rho}\right)_1(\rho uA)_1+(1-\eta_p)\dot{W}_t \tag{38}$$

Where the total energy is defined as

$$E=e+\frac{1}{2}u^2 \tag{39}$$

where e is the specific internal energy. In Eq. (38), η_p is the pump efficiency.

The pump head H is calculated as

$$H = \frac{\eta_p \dot{W}_t}{(\rho u A)_1 g} \tag{40}$$

where g is the gravitational constant.

The pump torque is calculated according to a scaling law as used in the Sandia model:

$$T_{pump} = \frac{T_{p0}}{\omega_0^2}\omega^2 \tag{41}$$

where T_{p0} and ω_0 are the rated pump torque and speed, respectively.

Pressures at the inlet and outlet pipe ends are calculated with the incompressible flow Bernoulli equation. We assume that the pump work is added to the fluid only in the entrance segment and the loss in the exit segment is ignored. For normal flow

$$p_1 = \left(p_J + \frac{1}{2}\rho_J u_J^2\right) - \rho_1 g H - \frac{1}{2}\rho_1 u_1^2 \tag{42}$$

$$p_2 = \left(p_J + \frac{1}{2}\rho_J u_J^2\right) - \frac{1}{2}\rho_2 u_2^2 \tag{43}$$

where

$$\rho_J = \rho(p_J, T_J) \tag{44}$$

$$u_J = \frac{(\rho u A)_1}{\rho_J A_J} \tag{45}$$

where A_J is the pump reference cross section area.

Downstream total energy is calculated by

$$(\rho E)_2 = \rho_2 \left(e(p_J, T_J) + \frac{1}{2}u_2^2\right) \tag{46}$$

3. BENCHMARK, VALIDATION AND TESTS

3.1 Convergent-Divergent Nozzle Tests

3.1.1 Nozzle Experiments With Pure Steam at Inlet

In our previous report [1], the same steam nozzle experiment used for benchmark in the Sandia research [2] was used for validating the proposed single-phase Terry turbine nozzle analytical model and comparing with Sandia CFD results. Here we add the two-phase Terry turbine nozzle model results to compare with experimental data and results from other models. Figure 4 shows the test nozzle geometry. This nozzle test only covers in-nozzle velocity data. Dry saturated steam is assumed at the nozzle inlet. The steam temperature is at saturation for the inlet pressure.

Figure 5 compares the velocity values calculated with the analytical models against the CFD results from the Sandia team and test data. Note that the nozzle test data reflects conditions just before the exit (near 90% nozzle length) while all the calculation results are at the nozzle exit. All of the analytical model results match the CFD results very well and both the analytical model results and the CFD results agree reasonably well with the test data except for the low-pressure steam jet test point. The reason for this discrepancy is due to the fact that shocks develop in the divergent section of the nozzle for the lower inlet pressure cases as revealed by the test data and CFD simulations. The simple analytical models cannot account for the situation in which shocks appear inside the nozzle. Shocks in the divergent section are indicative of over-expanded nozzle flow, which results from too low of a pressure drop over the nozzle geometry. However, over-expanded flow is not anticipated for the Terry turbine nozzles, given the high reactor vessel (or steam generator) pressures for such applications. Higher inlet pressures will push shocks out of the nozzle and result in under-expanded flow [2]. The two-phase analytical models predict slightly higher velocity values than the single-phase model. The results from the IHEM and Moody's models are very close. From the test nozzle benchmark, we conclude that the analytical models can predict nozzle exit velocities with accuracies similar to those obtained from complex CFD models.

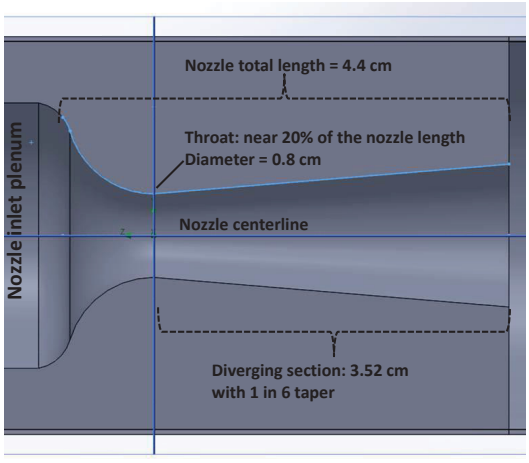

Figure 4. Test nozzle geometry [2].

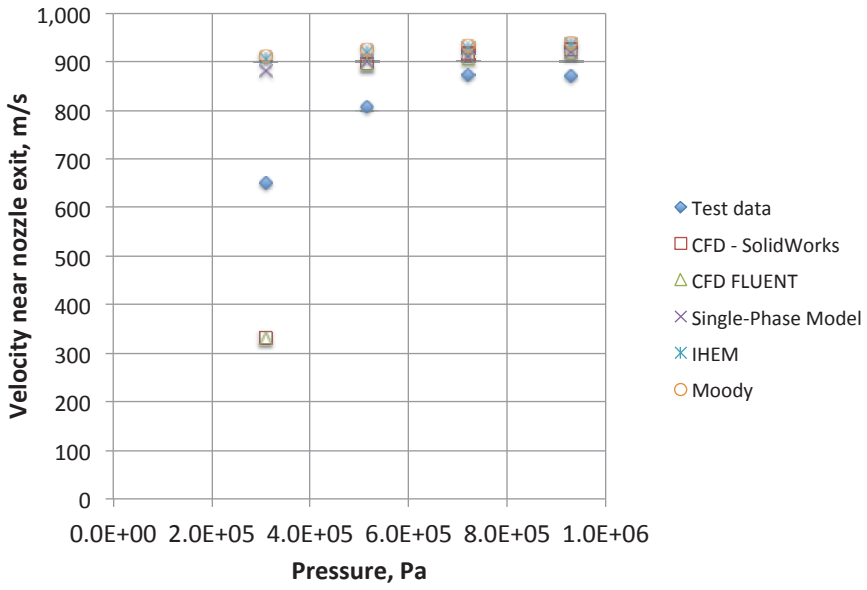

Figure 5. Velocities near test nozzle exit.

3.1.2 Terry Turbine Nozzle With Pure Steam at Inlet

The Terry turbine geometry specified by the Sandia study [2], as shown in Table 1, was used for the single-phase Terry turbine model benchmark study [1]. In this sub-section, the Sandia CFD results will be used for benchmarking the two-phase analytical nozzle model.

Figure 6 shows the choked mixture mass flow rates through the nozzle under different upstream pressures from different models. The single-phase analytical model predicts the highest choking flow rates while the Sandia CFD model predicts the lowest choking flow rates; the relative errors between the two models are about 10%. The two two-phase nozzle models – IHEM and Moody – predict results within the ranges of the CFD model and the single-phase nozzle model. Moody's model has slightly higher values than the IHEM model as expected. This error range should be within the uncertainty range for all the discussed methods. Figure 7 compares the mixture mass flow rate and the steam mass flow rates at the nozzle exit for IHEM and Moody models. Even though at the nozzle inlet only pure dry steam exists, the two-phase nozzle models show that there is a small amount of moisture at the exit of the nozzle, similarly predicted by the Sandia CFD simulations. The steam mass flow rates at the exit obtained from the IHEM and Moody models are quite close. It should be emphasized that the steam mass flow rate, not the mixture mass flow rate, is used to drive the turbine rotor in our Terry turbine model.

Table 1 Terry turbine geometry [2]

Model variable	Quantity
Turbine wheel diameter	61 cm (24 inches)
Turbine wheel and bucket width	7 cm
Number of nozzles and reversing chamber sets	5
Number of reversing chambers per nozzle set	4
Number of buckets on wheel	84
Nozzle length	1.7 cm
Nozzle circular throat diameter	0.56 cm
Nozzle square exit side length	0.64 cm
Distance from nozzle exit to bucket entrance	≈1.5 cm

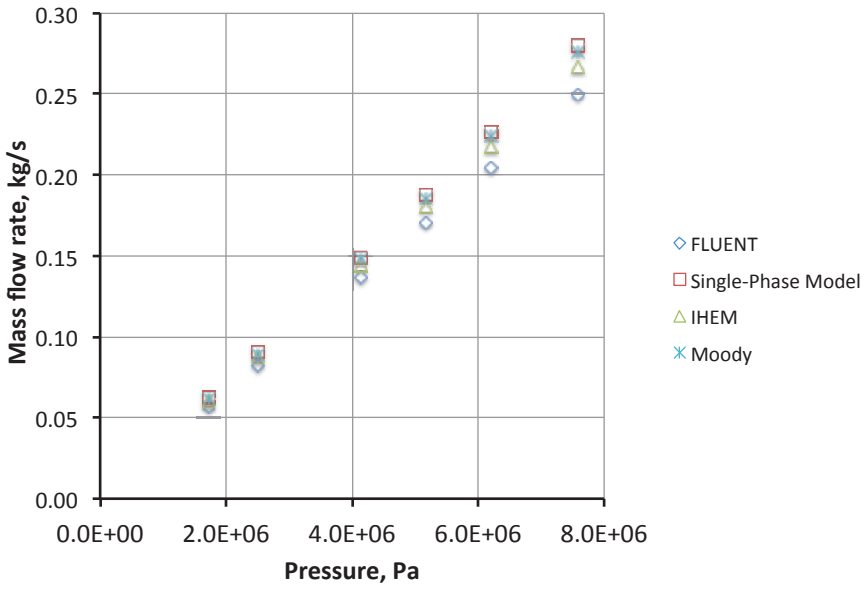

Figure 6. Choked mixture mass flow rates through the nozzle from different models.

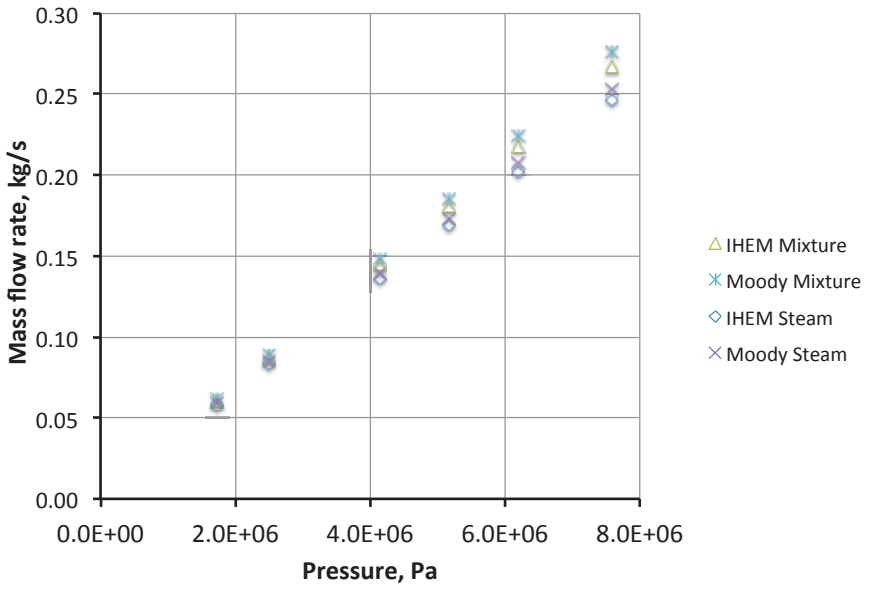

Figure 7. Mass flow rates through the nozzle for two-phase nozzle models.

Figure 8 and Figure 9 show the bucket entrance velocities for two different outlet pressures. The analytical nozzle models generally predict higher entrance velocities than the Sandia CFD model. The two-phase nozzle models predict lower velocities than the single-phase nozzle model and therefore the two-phase nozzle model results are closer to the CFD results. The IHEM and Moody models predict very similar bucket entrance velocities. For the high inlet pressure operation range typical for RCIC turbines (6 – 8 MPa), the two-phase nozzle models and CFD results are close: less than 10% difference for the high outlet pressure case and less than 5% for the low outlet pressure case. When the inlet pressure is lower than 5 MPa, the difference between the analytical models and the Sandia CFD model predictions becomes larger. However, both models predict similar trends. The RCIC system typically only experiences low inlet pressures during the short period of the primary system depressurization process. The RCIC system behavior is not important to the system response during depressurization due to the high rate of steam release through SRVs (Safety/Relief Valve) during this time. Considering these facts, the larger difference in the bucket entrance velocity for the lower inlet pressure cases should not be a big concern in term of the overall RCIC simulation uncertainty.

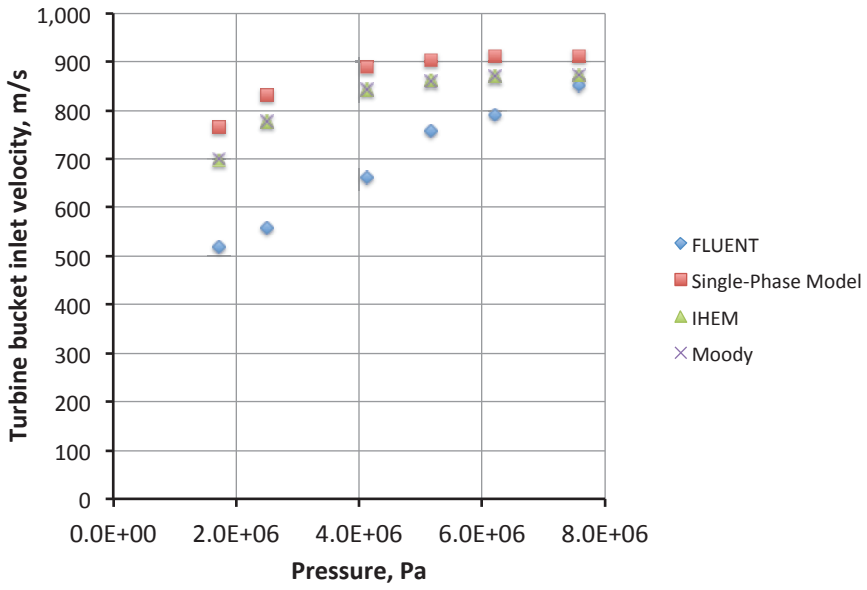

Figure 8. Turbine bucket inlet velocity for the high outlet pressure case (300 kPa).

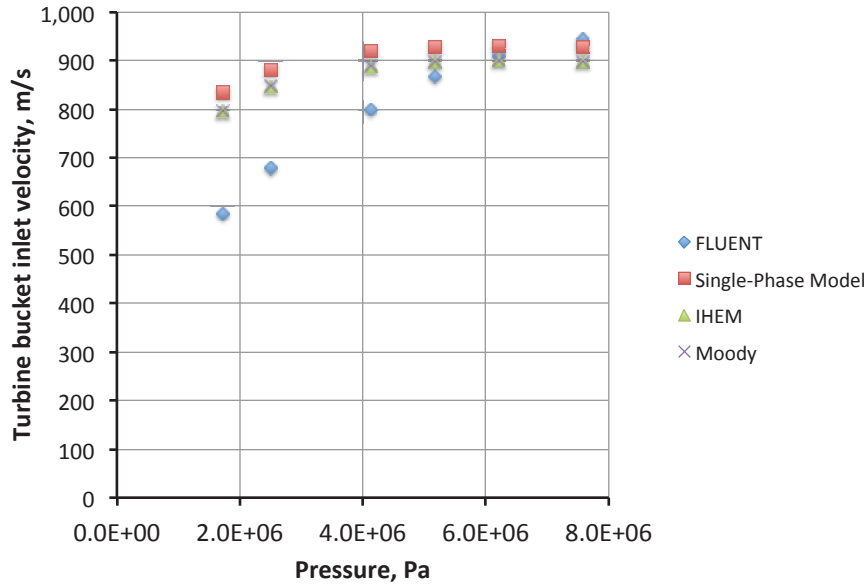

Figure 9. Turbine bucket inlet velocity for the low outlet pressure case (193 kPa).

3.2 RCIC System Tests

3.2.1 Start-up Test

The same RELAP-7 input model used for testing the single-phase Terry turbine model as shown in Figure 10 was used to test the two-phase Terry turbine system model. The input model is composed of a Terry turbine model, a coupled pump, a check valve on the water line, connecting pipes and time dependent

volumes at the boundaries. The boundary conditions are also shown in the figure. Two different turbine outlet pressures at 193 kPa and 300 kPa as used for the Terry turbine nozzle test are used in the simulations. The two-phase model simulation results are compared to the nominal steady state values and single-phase results.

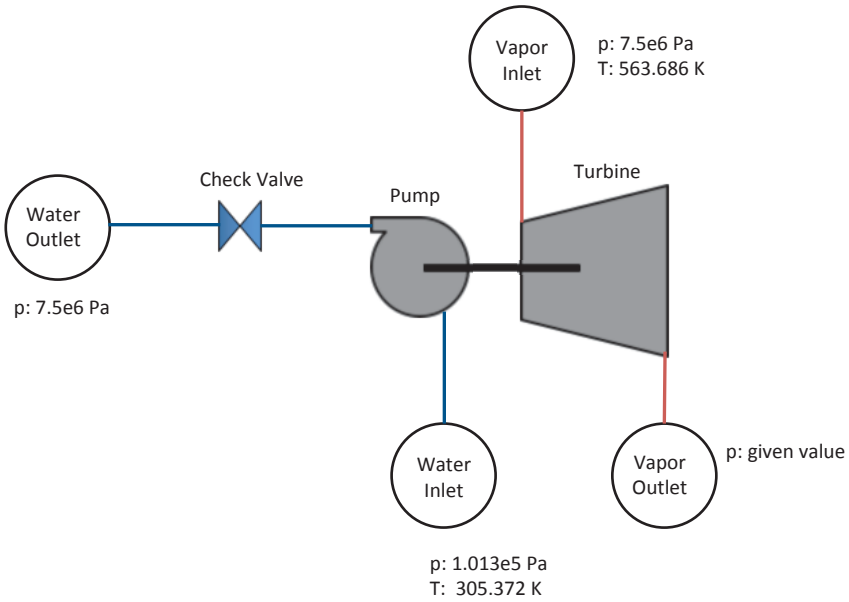

Figure 10. RELAP-7 Terry turbine RCIC system test model.

Table 2 shows the major parameters for the turbine and pump. These values are taken from the Sandia MELCOR test case which is based on a RCIC system for a generic 2000 MWt BWR [2]. Note that the rated pump head is not an input parameter. Since both the impulse conversion coefficient and the pump efficiency are not known, we use two known conditions to find out their best fits for the model at the turbine outlet pressure 193 kPa:

- The rated turbine speed and torque;
- The water mass flow rate through the pump is about 10 times the steam mass flow rate through the turbine.

The two parameters are then fixed for the other turbine outlet condition.

The simulation was run for 100 s to reach steady state. The time step in the beginning is 0.001 s, and gradually increases to 0.01 s at 10 s and maintains this value. The nozzle parameters rapidly achieve steady state values. Other major parameters of interest such as the shaft work, rotational speed, and pump torque take more than 1 minute to reach steady state. Table 3 and Table 4 compare important steady-state results from the two-phase models, single-phase model, Sandia model, and rated nominal values for the turbine outlet pressures at 193 kPa and 350 kPa, respectively. All models results are quite close to the rated values. The two-phase model with Moody's choking model produces closer results to the single-phase model than the IHEM choking model. Comparing results between two different outlet-pressure conditions, a higher outlet pressure results in a slower shaft speed, less torque, less shaft work, and a smaller pump mass flow rate for all the models; but the difference is not large. The calculated RCIC rotational speed at steady state from the Moody model is 444 radians/s, which is very close to the rated speed of 450 radians/s shown in Table 2. The calculated pump torque at steady state from the Moody model is 436 N-m, again very close to the rated value of 449 N-m. The calculated steady-state shaft work from the Moody model is very close to the rated value: 194 kW versus 202 kW (450 radians/s × 449 N-m). The mass flow rate through the pump is about 10 times as the rate through the turbine at

steady state, which is the expected ratio for a typical RCIC system [12]. The steam quality at the nozzle exit from both two-phase models is about 0.92.

Table 2 Terry turbine and pump parameters

Model Parameters	Value
Turbine wheel radius (r)	0.3 m
Turbine inlet/outlet angle (β)	π/4 radians
Number of nozzles	5
Total nozzle throat area	1.2315e-4 m^2
Total nozzle exit area	2.048e-4 m^2
Turbine moment of inertia (I)	10 kg-m^2
Impulse conversion coefficient (c_{IC})	1.1
Rated RCIC speed (ω_0)	450.295 radians/s (4300 rpm)
Rated pump torque (T_{p0})	449 N-m
Pump efficiency (η_p)	0.52
Rated pump head	766 m (7.52 MPa)

Table 3 Important Terry turbine and pump calculated parameters at steady state for outlet pressure at 193 kPa

Model Parameters	Rated Value	Modified Sandia Model	INL Model (Pure Steam)	INL Model (IHEM)	INL Model (Moody)
Pump efficiency	N/A	0.49	0.52	0.52	0.52
Turbine impulse conversion coefficient	N/A	N/A	0.98	1.1	1.1
Pump head, m	766.	755.	755.	755.	755.
RCIC speed, rad/s	450.	455.	446.	438.	444.
Pump torque, N-m	449.	459.	441.	425.	436.
Shaft work, kW	202.	209.	197.	186.	194.
Bucket entrance speed, m/s	N/A	946.	928.	908.	907.
Turbine mass flow rate, kg/s	N/A	1.39	1.39	1.32	1.36
Pump mass flow rate, kg/s	N/A	13.83	13.84	13.09	13.61

Table 4 Important Terry turbine and pump calculated parameters at steady state for outlet pressure at 300 kPa

Model Parameters	Rated Value	Modified Sandia Model	INL Model (Pure Steam)	INL Model (IHEM)	INL Model (Moody)
Pump efficiency	N/A	0.49	0.52	0.52	0.52
Turbine impulse conversion coefficient	N/A	N/A	0.98	1.1	1.1
Pump head, m	766.	755.	755.	755.	755.
RCIC speed, rad/s	450.	427.	442.	432.	437.
Pump torque, N-m	449.	403.	433.	412.	423.
Shaft work, kW	202.	172.	192.	178.	185.
Bucket entrance speed, m/s	N/A	841.	913.	883.	882.
Turbine mass flow rate, kg/s	N/A	1.39	1.39	1.32	1.36
Pump mass flow rate, kg/s	N/A	11.39	13.47	12.51	12.98

3.2.2 RCIC System Test With Periodic Inlet Condition

A RCIC system test with a periodic steam quality inlet condition has been developed based on the model shown in Figure 10 in order to test the two-phase Terry turbine model. The turbine inlet pressure is 7.5 MPa and the turbine outlet pressure is 193 kPa. The steam quality at the turbine inlet as shown in Figure 11 is inputted through a control file. The goal is to create a Fukushima-accidents-like scenario, with a reasonable self-regulating behavior appearing in the simulation. Both IHEM and Moody two-phase models are used. The simulation covers about two cycles of dry-flood stages. A quick transition period of 20 seconds is assumed between dry steam turbine inlet and pure water turbine inlet conditions.

As shown in Figure 12 for the IHEM model results, the mass flow rate through the pump minus the mixture mass flow rate through the turbine is the net water addition to the reactor vessel. In the dry stage, water is added to the reactor vessel; and in the flooded stage, the water is removed from the reactor vessel. Therefore, decay heat can be continuously removed by the RCIC system from the reactor core to the suppression pool in this postulated self-regulation mode. Figure 13 shows very similar mass flow rate results using the Moody model. Both the mass flow rates through the turbine and pump from the Moody model are higher than the predictions from the IHEM model.

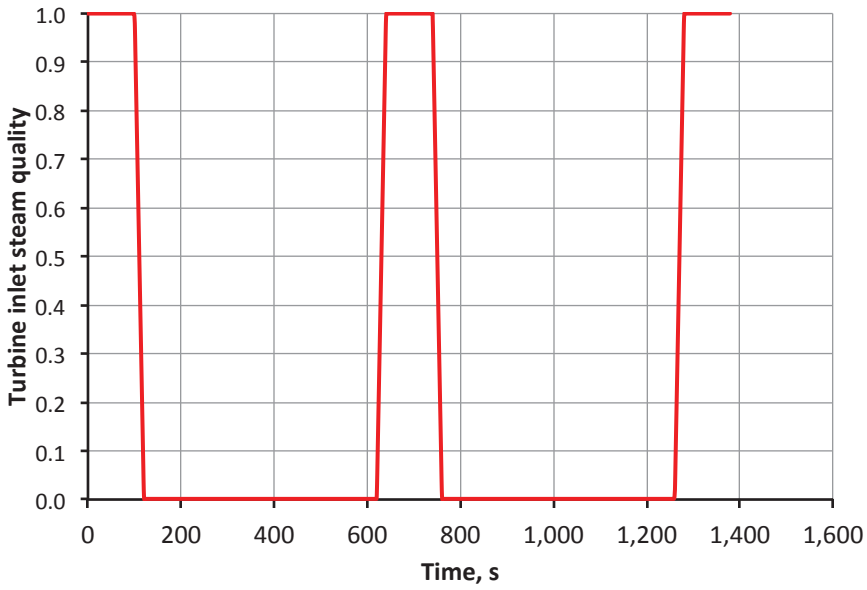

Figure 11. Specified turbine inlet steam quality for the RCIC system simulation with periodic inlet condition.

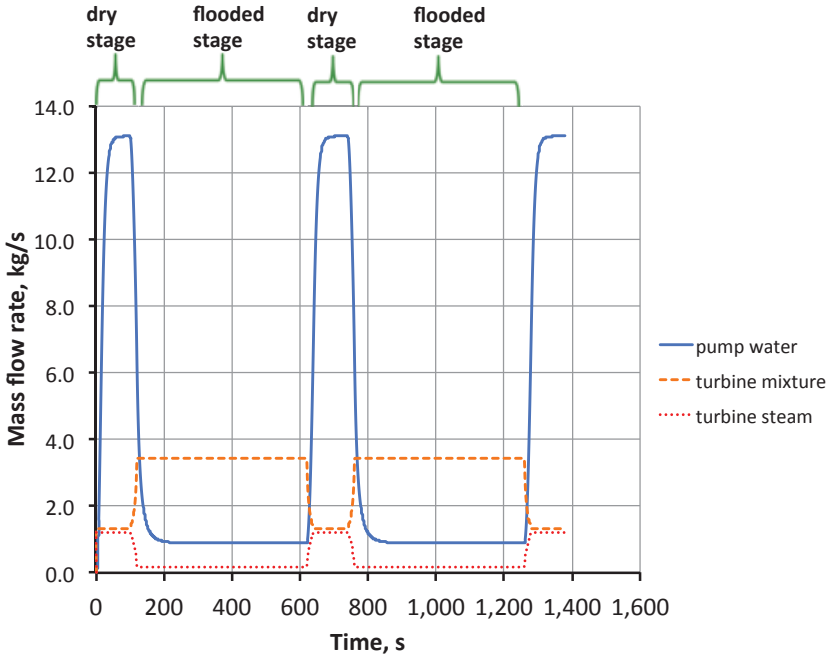

Figure 12. Calculated mass flow rates through the RCIC – mixture and steam through the turbine nozzle exit, water through the pump for the RCIC system simulation with periodic inlet condition with the IHEM model.

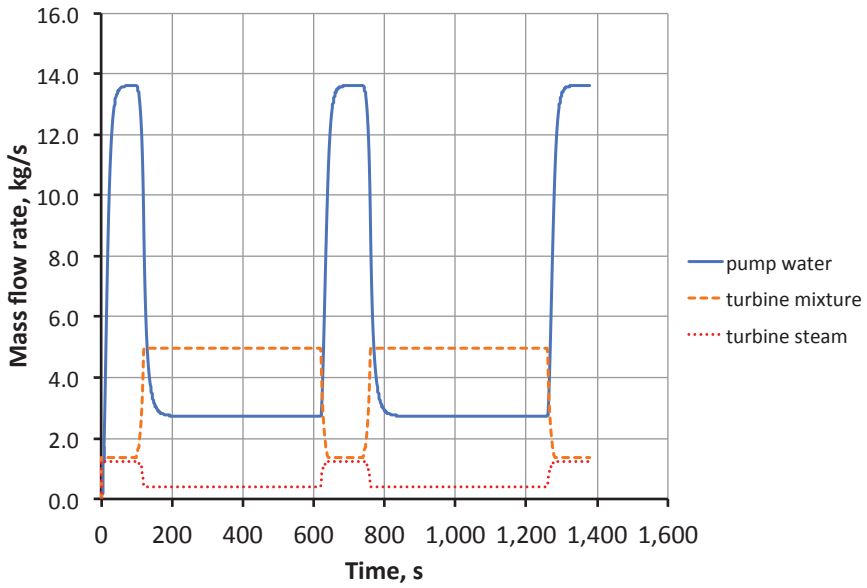

Figure 13. Calculated mass flow rates through the RCIC – mixture and steam through the turbine nozzle exit, water through the pump for the RCIC system simulation with periodic inlet condition with the Moody model.

Figure 14 to Figure 16 show the calculated turbine shaft work, rotational speed, and pump torque from the IHEM and Moody models, respectively. Moody's model predicts higher values than the IHEM does; and the difference is larger in the flooded stage than in the single-phase steam space. This can be explained by recalling that the IHEM model predicts the lowest choking flow rate among all the two-phase choking models.

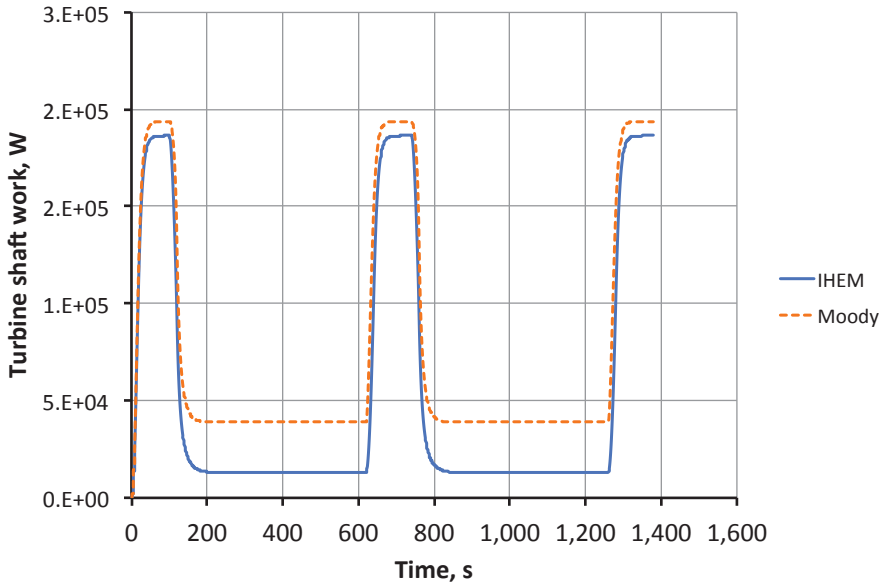

Figure 14. Calculated turbine shaft work for the RCIC system simulation with periodic inlet condition.

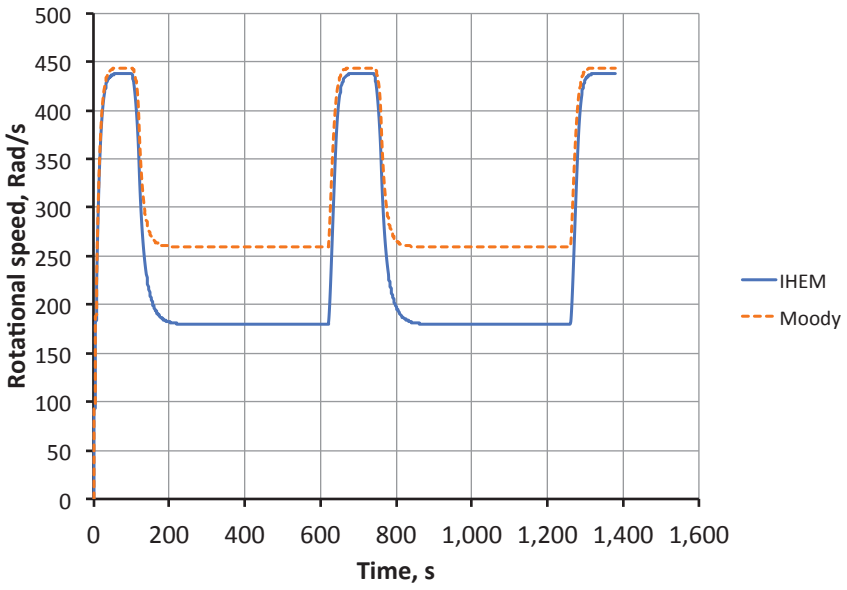

Figure 15. Calculated rotational speed for the RCIC system simulation with periodic inlet condition.

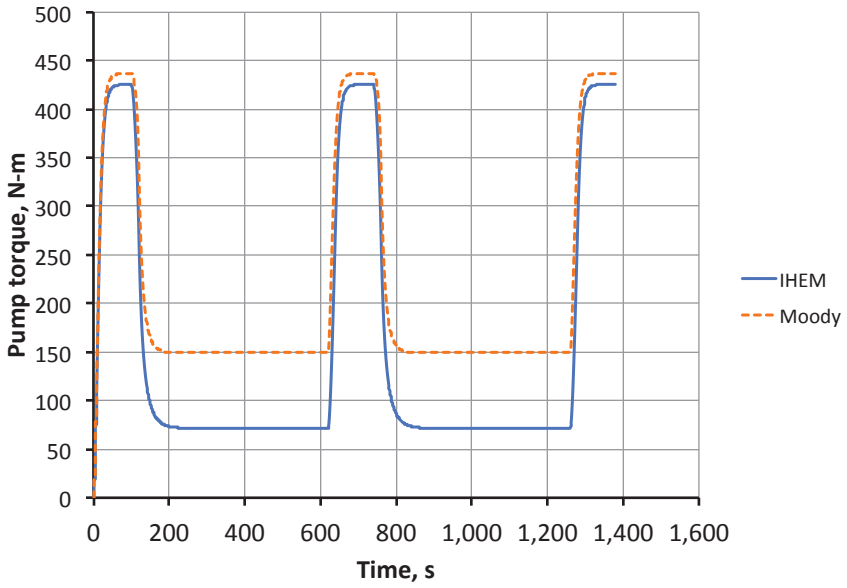

Figure 16. Calculated pump torque for the RCIC system simulation with periodic inlet condition.

Figure 17 to Figure 20 show calculated pressure, steam quality, void fraction and sound speed at the turbine nozzle throat, respectively. The IHEM model has much higher throat pressure than the Moody model for the low-steam inlet conditions. The steam qualities at the throat from the two models only have a small difference. With the pure water inlet condition, the steam quality at the throat is low. However, even with the pure water inlet condition, the void fraction at the nozzle throat is quite high from both models. The IHEM model results in higher throat void fractions than Moody model. The predicted sound speeds at the throat obtained from the two models are quite different, with IHEM model resulting very low sound speeds in the strong two-phase regions.

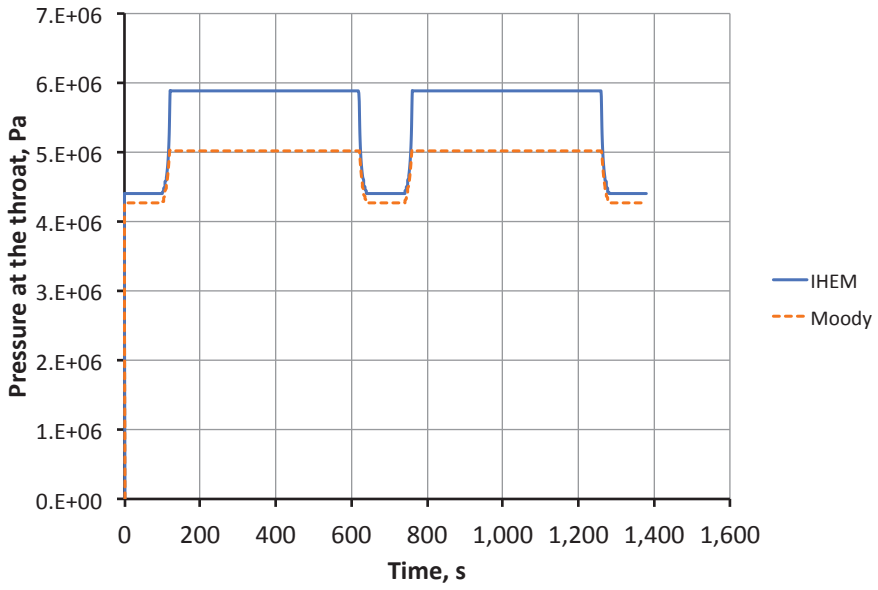

Figure 17. Calculated pressure at the turbine nozzle throat for the RCIC system simulation with periodic inlet condition.

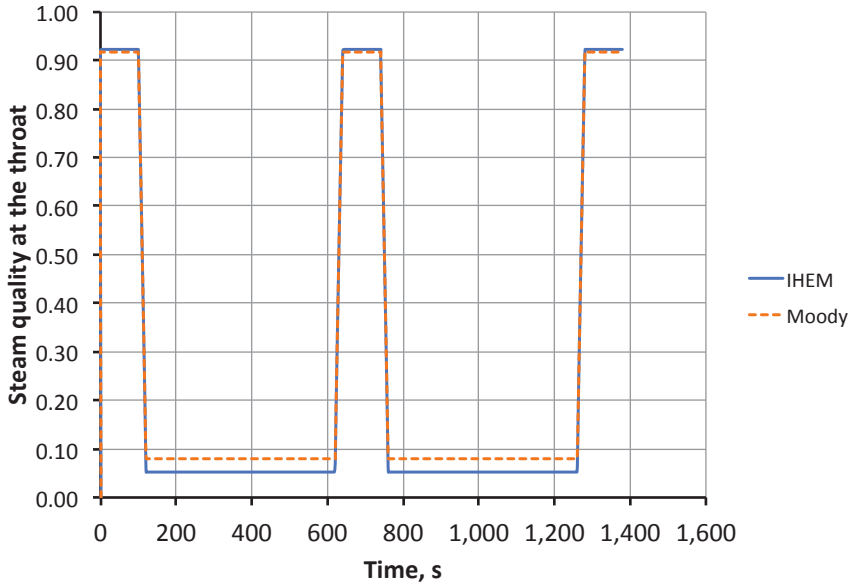

Figure 18. Calculated steam quality at the turbine nozzle throat for the RCIC system simulation with periodic inlet condition.

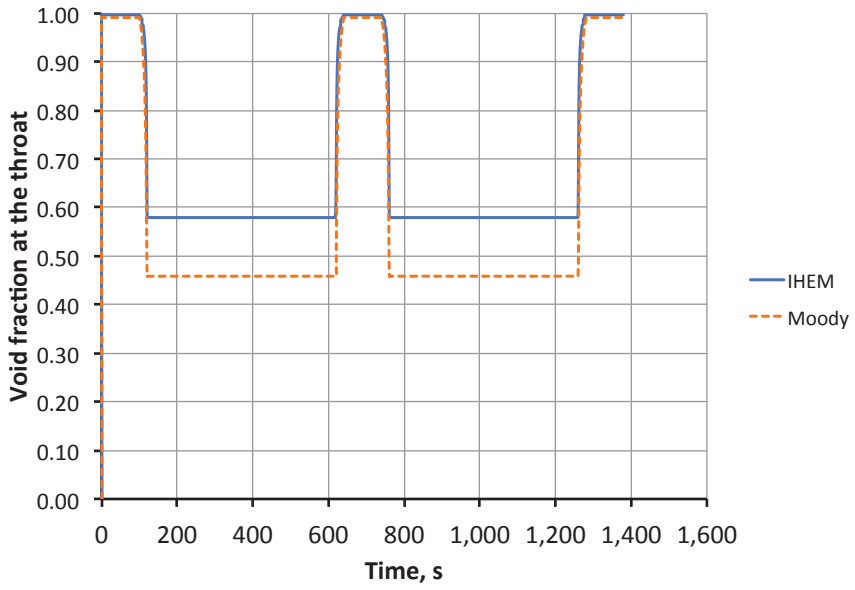

Figure 19. Calculated void fraction at the turbine nozzle throat for the RCIC system simulation with periodic inlet condition.

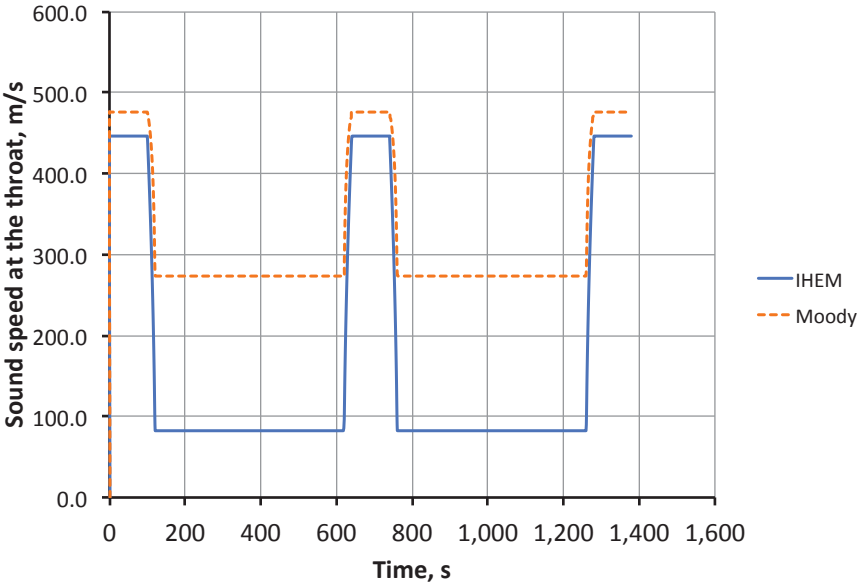

Figure 20. Calculated sound speed at the turbine nozzle throat for the RCIC system simulation with periodic inlet condition.

Figure 21 to Figure 23 show important results at the turbine nozzle exit. These results strongly depend on the assumed two-phase expansion model between the nozzle throat and the exit. In this work, we assume a frozen model and a perfect ideal gas expansion process for the vapor phase. These two models should result in the largest potential expansion or pressure drop. If phase interaction and non-isentropic expansion were considered, lower pressure drops would be predicted. However, for all different nozzle expansion models, the mixture pressure will drop to the turbine bucket ambient pressure through the free expansion stage. The effects of different in-nozzle expansion models on the overall Terry turbine model

performance should be limited. The differences between IHEM and Moody models are not large for the nozzle exit pressure, void fraction, and steam velocity. Figure 24 shows the steam bucket entrance velocity. The velocities from the two models are quite close and vary in narrow ranges during the whole transient. The large variation of the Terry turbine performance during the transient is therefore dominantly caused by the variation of the vapor mass flow rate.

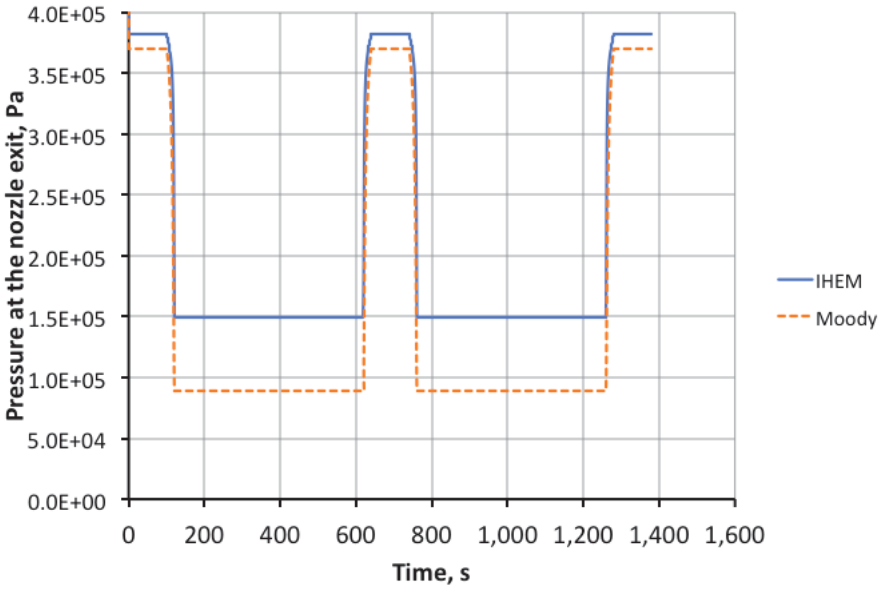

Figure 21. Calculated pressure at the turbine nozzle exit for the RCIC system simulation with periodic inlet condition.

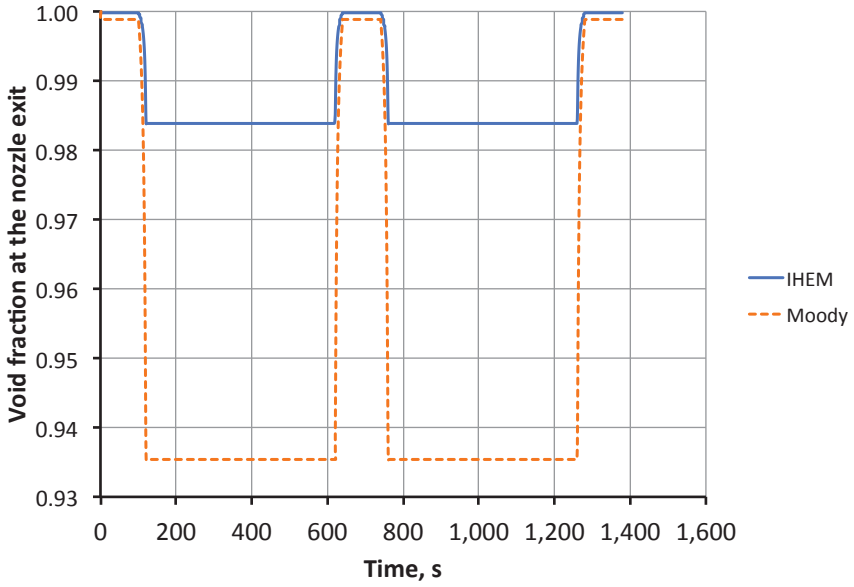

Figure 22. Calculated void fraction at the turbine nozzle exit for the RCIC system simulation with periodic inlet condition.

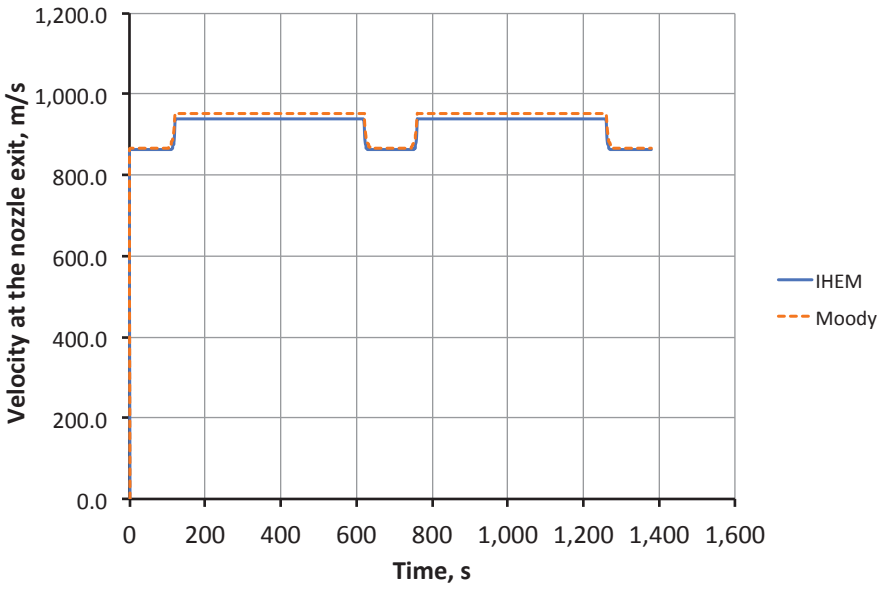

Figure 23. Calculated velocity at the turbine nozzle exit for the RCIC system simulation with periodic inlet condition.

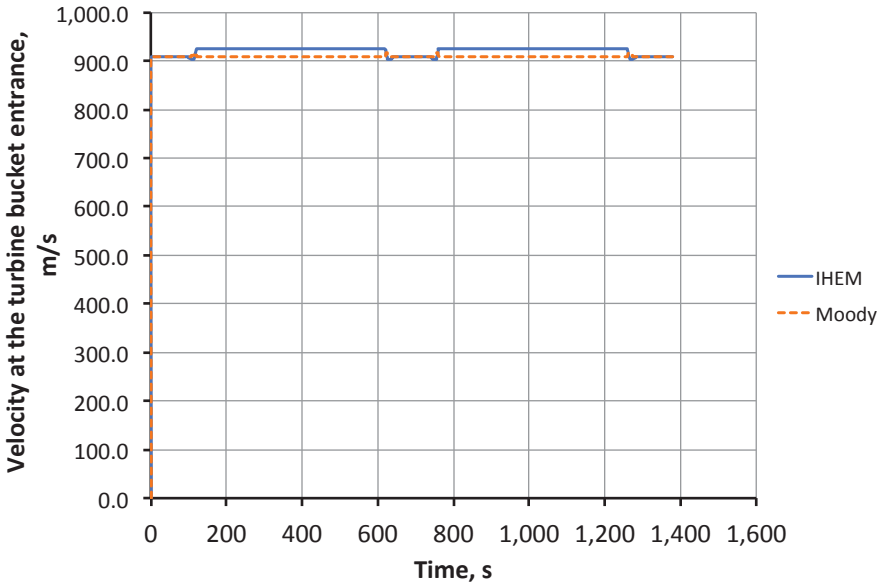

Figure 24. Calculated velocity at the turbine bucket entrance for the RCIC system simulation with periodic inlet condition.

4. SUMMARY

In this work, we present a complete set of two-phase analytical models for the Terry turbine system, based on our previous work on the single-phase analytical model. The whole system consists of a Terry turbine model and a pump model. The Terry turbine model is composed of a nozzle model and a turbine rotor model. The nozzle model is further divided into three parts: (1) expansion and chocking models from the nozzle inlet to the throat, (2) expansion in the divergent section of the nozzle, and (3) the free expansion stage between the nozzle exit to the turbine bucket entrance. For the expansion model in the convergent section of the nozzle, two classic two-phase choking models - Isentropic Homogenous Equilibrium Model (IHEM) and Moody's model are included. The two choking models provide bounding cases for the two-phase choking flow rate. The new two-phase Terry turbine model uses the choking models to calculate the mass flow rate, the critical pressure at nozzle throat, and steam quality. In the divergent stage, we only consider the steam phase with a similar model as that used for the single-phase case by assuming that the liquid phase would slip along the wall with a much slower speed and will not contribute the impulse on the rotor. We also modify the stagnation conditions according to two-phase choking conditions at the throat and the cross-section areas for steam flow at the throat and at the nozzle exit.

The new two-phase Terry turbine model has been tested with RELAP-7 and was benchmarked with the same steam nozzle tests as for the single-phase model. Better agreement with the Sandia CFD results for the pure steam inlet Terry nozzle test is observed than from the single-phase model. The RCIC start-up tests with two-phase models were also simulated and compared with the single-phase model. Similar results are obtained. Finally, we designed a new RCIC system test case to simulate the self-regulated Terry turbine behavior observed in Fukushima accidents. In this test, a period inlet condition for steam quality varying from 1 to 0 was applied. For the dry steam inlet period, the RCIC system behaves just like the normal operation condition, with a high pump injection flow rate and a nominal steam release rate through the turbine, resulting in the net addition of water to the primary system; for the flooded inlet period, the RCIC turbine shaft work dramatically decreases and results in a much reduced pump injection flow rate and an increased mixture flow rate out of the turbine. The net effect for this period is removal of coolant from the primary loop. With the periodic addition and removal of coolant to the primary loop, the self-regulation mode of the RCIC system can be maintained for a quite long time. Both IHEM and Moody's models generate similar phenomena; however, noticeable differences can be observed.

This work represents the first step for two-phase Terry turbine analytical models. The preliminary models can be refined with more local modeling choices. The near future work should be focused on using Terry turbine test data to validate the proposed models when the data become available. Additional model refinement will also be pursued, such as trying additional choking models and investigating different nozzle expansion models in the nozzle divergent section, adding homologous curves for the pump, and developing thermal mixing and stratification models for the wet well.

5. REFERENCES

1. H. Zhao, et. al., *Development and Implementation of Mechanistic Terry Turbine Models in RELAP-7 to Simulate RCIC Normal Operation Conditions*, INL/EXT-16-39857, rev 1, January 2017.
2. K. Ross, et. al., Modeling of the Reactor Core Isolation Cooling Response to Beyond Design Basis Operations – Phase 1, SAND2015-10662, December, 2015.
3. R. Gauntt, et. al., "Fukushima Daiichi Accident Study (Status as of April 2012)," SAND2012-6173, Sandia National Laboratories, Albuquerque, NM, August 2012.
4. R.T. Lahey, Jr. and F.J. Moody, The thermal-Hydraulics of A Boiling Water Nuclear Reactor, 2nd edition, American Nuclear Society, 1993.
5. F.J., Moody, "Maximum Flow Rate of a Single-Component, Two-Phase Mixture," Transactions of the ASME, Journal of Heat Transfer, Vol. 88, pp. 134-141, 1965.
6. S. Levy, Two-phase flow in complex systems. John Wiley & Sons, page 303 to 305, 1999.
7. J. Kiefer, "Sequential minimax search for a maximum", Proceedings of the American Mathematical Society, 4 (3): 502–506, 1953.
8. Y.A. Cengel and J.M. Cimbala, *Fluid Mechanics: Fundamentals and Applications*, Third Edition, Mc Graw Hill, 2014.
9. K. Bulent Yuceil and M. Volkan Otugen, "Scaling Parameters for Underexpanded Supersonic Jets," *Physics of Fluids*, **14**, 4206, 2002.
10. J. Xiao, J. R. Travis, W. Breitung, "Hydrogen release from a high pressure gaseous hydrogen reservoir in case of a small leak," International Journal of Hydrogen Energy, 36, 2545-2554, 2011.
11. A. Velikorodny and S. Kudriakov, "Numerical Study of the Near-Field of Highly Under-Expanded Turbulent Gas Jets", Proc. of ICHS 2011, 2011.
12. H. Lopez, et al., "RELAP RCIC Pump Homologous Curves Generation and Verification for Fukushima Unit 2," *Transactions of the American Nuclear Society*, **Vol. 111,** 2014.